

# Quantum path integral simulation of isotope effects in the melting temperature of ice Ih

R. Ramírez and C. P. Herrero

*Instituto de Ciencia de Materiales de Madrid (ICMM),*

*Consejo Superior de Investigaciones Científicas (CSIC), Campus de Cantoblanco, 28049 Madrid, Spain*

The isotope effect in the melting temperature of ice Ih has been studied by free energy calculations within the path integral formulation of statistical mechanics. Free energy differences between isotopes are related to the dependence of their kinetic energy on the isotope mass. The water simulations were performed by using the q-TIP4P/F model, a point charge empirical potential that includes molecular flexibility and anharmonicity in the OH stretch of the water molecule. The reported melting temperature at ambient pressure of this model ( $T=251$  K) increases by  $6.5\pm0.5$  K and  $8.2\pm0.5$  K upon isotopic substitution of hydrogen by deuterium and tritium, respectively. These temperature shifts are larger than the experimental ones (3.8 K and 4.5 K, respectively). In the classical limit, the melting temperature is nearly the same as that for tritiated ice. This unexpected behavior is rationalized by the coupling between intermolecular interactions and molecular flexibility. This coupling makes the kinetic energy of the OH stretching modes larger in the liquid than in the solid phase. However the opposite behavior is found for intramolecular modes, which display larger kinetic energy in ice than in liquid water.

PACS numbers: 64.70.dj, 82.20.Wt, 64.70.D-, 65.20.De

## I. INTRODUCTION

Quantum mechanical effects associated to the nuclear mass play a significant role in the properties of liquid water and ice. Experimental evidence is provided by the isotope dependence of the equilibrium properties of water. At ambient pressure the melting point at 273.15 K increases by 3.8 K and 4.5 K after isotopic substitution of hydrogen by deuterium or tritium, respectively. An even larger isotope effect is found in the temperature ( $T=277.13$  K) of maximum density (TMD), that increases at ambient pressure by 7.2 K in heavy water and by 9.4 K in tritiated water. Such behavior can not be described by classical statistical mechanics, as in this limit the atomic masses do not affect the phase diagram of a substance or the equilibrium structure of a liquid. The importance of quantum effects related to the atomic masses in water might be expected by the presence of the lightest atom. However, the larger oxygen mass is also the origin of significant quantum properties of even practical relevance. For example, the isotopic composition of the annual layers of ice accumulated in the Antarctica has provided an indirect measure of the temperature of our planet over the last 400,000 years. The reason is that the vapor pressures of  $\text{H}_2^{16}\text{O}$ ,  $\text{H}_2^{18}\text{O}$ , and  $\text{D}_2^{16}\text{O}$  are different, and then the isotopic composition of ice results to be a function of the temperature at which it precipitated. Thus, isotope analysis in ice provides an historical record for climate change in the past.<sup>1</sup>

Computer simulation of water in clusters and condensed phases has attracted a lot of interest since the pioneering work of Barker and Watts<sup>2</sup> and Rahman and Stillinger<sup>3</sup> using rigid nonpolarizable models for the water molecule. Since then a lot of effort has been invested in the development and refinement of empirical potentials for both water and ice simulations. In fact, there appears

an embarrassing variety of them in the computer simulation literature. The most employed models assume a rigid geometry of the water molecule, some include molecular flexibility either with harmonic or anharmonic OH stretches, and another group deals explicitly with polarizability effects.<sup>4</sup> Moreover, in some cases slight modifications of the potential parameters are proposed for their use in quantum simulations, to avoid overcounting of quantum effects if the model parameters were first fitted against experimental data by classical simulations.<sup>5,6</sup> Besides, there is an increasing number of water simulations using *ab initio* density functional theory (DFT).<sup>7,8</sup> However, the H-bond network, with a strength between weak covalent and van der Waals interactions, seems difficult to be described with presently available energy functionals. As a result, some properties of ice may be poorly reproduced by DFT simulations, e.g., its melting temperature can be overestimated by more than 130 K.<sup>9</sup>

The melting point of ice at ambient pressure has been determined for the most common rigid models within the classical limit.<sup>10</sup> It was found that the TIP4P model, with melting point at  $T = 232$  K, results superior to other models in the sense that correctly predicts that ice Ih is the stable phase at ambient pressure, while the prediction of the other rigid models (SPC, SPC/E, TIP3P and TIP5P) was ice II. An improved parametrization of the rigid model (TIP4P/2005) displays a melting point at 251 K.<sup>11</sup> Quantum simulations of phase coexistence are less common than their classical counterparts. An exception is the work of Habershon *et al.*,<sup>12</sup> who have developed a flexible water model (q-TIP4P/F) by adding to the rigid TIP4P/2005 potential the intramolecular flexibility with the help of OH Morse-type stretches. The model was parametrized on the basis of quantum path integral (PI) simulations. Its melting point at 251 K and ambient pressure, was derived by direct coexistence PI simulations of

the water-ice interface. Moreover, in the classical limit the melting point was found just 8 K above the quantum result. This temperature shift was considered consistent with the experimental difference of 4 K between the melting points of  $\text{H}_2\text{O}$  and  $\text{D}_2\text{O}$ .<sup>12</sup> For the point charge flexible q-SPC/Fw model<sup>13</sup> the classical melting point was however found about 27 K higher than the quantum result of 195 K.<sup>12</sup> This difference in the quantum correction of both models might be originated from the description of the intramolecular OH stretches, i.e., anharmonic (q-TIP4P/F) versus harmonic (q-SPC/Fw) OH vibrations.

Although the determination of quantum corrections to classical melting points is interesting because it allows us to quantify the systematic error of treating water molecules as classical entities, they do not represent any kind of measurable property. There is no way to perform measurements of the phase behavior of water in the classical limit. In this respect, the calculation of the isotope effect in the melting point of ice offers the advantage of being directly comparable to experimental data, providing a better test of the capability of the water model. We are not aware of previous computer simulations of this isotope effect. However, by the quantum cluster equilibrium theory, that calculates equilibrium properties by extending standard quantum statistical thermodynamics of chemical equilibrium to the analogous equilibrium between molecular clusters, it was estimated that the melting point of  $\text{D}_2\text{O}$  is shifted by about 2 K towards higher temperatures with respect to light water.<sup>14</sup> Isotope effects have been studied by PI simulations in many other equilibrium properties of water. Kuharski and Rossky found that the liquid  $\text{H}_2\text{O}$  is less structured than  $\text{D}_2\text{O}$ .<sup>15</sup> The explanation was formulated in terms that the quantum effect associated to the lower isotope mass results in a less structured H-bond network and a less tightly bound liquid.<sup>16,17</sup> Other simulations of isotope effects focused on the TMD<sup>4,18</sup>, the diffusion coefficient,<sup>19,20</sup> the heat capacity,<sup>21,22</sup> and the infrared spectra<sup>20</sup> of water.

In this paper we present a PI simulation of the isotope effect in the melting temperature of ice Ih at ambient pressure. The q-TIP4P/F model has been chosen for the simulations because it is an anharmonic flexible potential whose normal melting point has been already established by quantum PI simulations.<sup>12</sup> Thus, assuming the equality of the Gibbs free energy,  $G$ , of ice Ih and water at the melting point, the isotope effect will be calculated from the dependence of  $G$  with isotope mass and temperature. Solid-liquid coexistence will be also studied in the classical limit. The calculation of  $G$  will be performed using adiabatic switching (AS) (Ref. 23) and reversible scaling (RS) (Ref. 24) approaches, that are based on algorithms where a Hamiltonian parameter (e.g., an atomic mass) or a state variable (e.g., the temperature) changes along a non-equilibrium simulation run. The capability of both AS and RS methods to calculate free energies in the context of PI simulations has been recently analyzed in the study of the phase diagram and isotope effects of neon.<sup>25,26</sup>

The structure of this paper is as follows. In Sec. II we present the computational conditions employed in the PI simulations as well as the techniques used to evaluate the free energy as a function of the isotope mass and temperature. In Sec. III, selected results of quantum simulations are compared to available data of Habershon *et al.*<sup>12</sup> and also to the classical limit as a check of the employed computational conditions. In particular, quantum and classical radial distribution functions (RDFs) of the liquid phase are presented in Subsec. III A, while the quantum and classical TMD of water at ambient pressure is summarized in Subsec. III B. The isotope effect in the melting temperature of ice is the focus of Sec. IV. Results obtained for  $\text{D}_2\text{O}$  and  $\text{T}_2\text{O}$  are compared to available experimental data in Subsec. IV A. The classical limit is presented in Subsec. IV B. The calculated isotope effects are rationalized by a discussion of the mass dependence found for the kinetic energy (KE) in Subsec. IV C. Finally, we summarize our conclusions in Sec. V.

## II. METHODOLOGY

### A. Computational conditions

In the PI formulation of statistical mechanics the partition function is calculated through a discretization of the integral representing the density matrix. This discretization defines cyclic paths composed by a finite number  $L$  of steps, that in the numerical simulation translates into the appearance of  $L$  replicas (or beads) of each quantum particle. Then, the implementation of PI simulations relies on an isomorphism between the quantum system and a classical one, derived from the former by replacing each quantum particle (here, atomic nucleus) by a ring polymer of  $L$  classical particles, connected by harmonic springs with a temperature- and mass-dependent force constant. Details on this computational method are given elsewhere.<sup>27–30</sup> The configuration space of the classical isomorph can be sampled by a molecular dynamics (MD) algorithm, that has the advantage against a Monte Carlo method of being more easily parallelizable, an important fact for efficient use of modern computer architectures. Effective reversible integrator algorithms to perform PI MD simulations in either  $NVT$  or  $NPT$  ensembles ( $N$  being the number of particles,  $V$  the volume,  $P$  the pressure, and  $T$  the temperature) have been described in detail in Refs. 31–34. Both isotropic and full cell fluctuations were programmed for the  $NPT$  ensemble. All calculations were done using originally developed software and parallelization was implemented by the MPI library.<sup>35</sup>

Simulations of water were performed on cubic cells containing 300 molecules, assuming periodic boundary conditions. Ice simulations included 288 molecules in an orthorhombic simulation cell with parameters  $(4a, 3\sqrt{3}a, 3c)$ , with  $(a, c)$  being the standard hexagonal lattice parameters of ice Ih. A proton disordered ice structure

where each O atom has two chemically bonded and two hydrogen bonded H atoms with nearly zero dipole moment of the simulation cell was generated by a Monte Carlo procedure.<sup>36</sup> Cell fluctuations in the extended dynamics of the  $NPT$  ensemble were isotropic for the liquid phase and flexible for the solid simulation cell. The point charge, flexible q-TIP4P/F model was employed for the simulations.<sup>12</sup> The Lennard-Jones interaction between oxygen centers was truncated at  $r_c=8.5$  Å, and standard long-range corrections were computed assuming that the pair correlation function is unity,  $g(r) = 1$  for  $r > r_c$ , leading to well-known corrections for the pressure and internal energies.<sup>37</sup> Long-range electrostatic interactions and forces were calculated by the Ewald method, and the calculation was speeded up by allowing the real and reciprocal space sums to be performed in parallel. The Gaussian smearing parameter in the Ewald method was set to 0.465 Å, so that both real and  $\mathbf{k}$ -space sums require similar computation time.

To have a nearly constant precision in the PI results at different temperatures, the number of beads  $L$  was set as the integer number closest to fulfill the relation  $LT=6000$  K, i.e., at 300 K the number of beads was  $L = 20$ . The classical limit is easily achieved within the PI algorithm by setting  $L=1$ . The staging transformation for the bead coordinates was employed for the quantum simulations. Temperature was controlled by chains of four Nosé-Hoover thermostats coupled to each of the staging variables, and in the case of the  $NPT$  ensemble an additional chain of four barostats was coupled to the volume.<sup>34</sup> To integrate the equations of motion, a reversible reference system propagator algorithm (RESPA) was employed.<sup>31</sup> For the evolution of thermostats and harmonic bead interactions a time step  $\delta t = \Delta t/4$  was used, where  $\Delta t$  is the time step associated to the calculation of the q-TIP4P/F forces. A value of  $\Delta t=0.3$  fs was found to provide adequate convergence. The virial estimator was employed for the calculation of the KE,<sup>38,39</sup> and the pressure estimator was identical to that used in a previous work.<sup>40</sup> Typical runs consisted of  $5 \times 10^4$  MD steps (MDS) for equilibration, followed by runs using between  $5 \times 10^5$  and  $4 \times 10^6$  MDS for calculation of equilibrium properties. The longest runs were required for the liquid phase, in particular for the calculation of the water density as a function of temperature.

## B. Relative free energy

The thermodynamic integration is a standard technique that allows us to obtain free energy differences by the calculation of the reversible work needed to change the original system into a reference state of known free energy.<sup>41–43</sup> The Hamiltonian is switched along a path that connects both systems and a set of equilibrium simulations are performed at several points of this path. The AS method is an alternative procedure where the reversible work is estimated by slowly changing the system

Hamiltonian along a single non-equilibrium simulation run.<sup>23</sup> The RS algorithm was formulated to obtain free energies as a function of a state variable, typically  $T$  or  $P$ . In this case, a slow (adiabatic) change of the state variable is performed along the non-equilibrium simulation run.<sup>24</sup> Both AS and RS methods have been recently applied to study the phase diagram of neon by PI simulations.<sup>25,26</sup> Here we summarize how these methods fit into our calculation of the isotope effect in the melting temperature of ice.

The first step is to obtain the free energy of each phase (solid and liquid) at some appropriate reference point. The melting temperature of the q-TIP4P/F model for  $H_2O$  at normal pressure was estimated by Habershon *et al.* by PI simulations.<sup>12</sup> Hence this state point ( $T_R=251$  K,  $P_R=1$  atm) is a reference state where the Gibbs free energies of the solid,  $G_s$ , and the liquid,  $G_l$ , are identical. However, as the melting point was determined by direct coexistence, the actual value of the free energy remains unknown. This is not a limitation, as only free energy differences with respect to the reference state are needed for our purpose of calculating isotope shifts. In particular, free energy is required as a function of the hydrogen isotope mass,  $m_F$ , and temperature. Thus, without loss of generality, we set an arbitrary zero for the entropy,  $S_0$ , so that we will calculate at ambient pressure relative free energies,  $G_R$ , defined as

$$G_R(T, m_F) = G(T, m_F) - TS_0. \quad (1)$$

The pressure dependence of  $G$  is omitted here as it is a constant ( $P=1$  atm) for all simulations in this work. An alternative to our choice of setting an arbitrary zero of entropy would be to set an arbitrary zero for the Gibbs free energy. Both choices would be physically equivalent in the sense that they would lead to identical results for the phase coexistence temperature. However, the advantage of setting a zero of entropy is that then the temperature dependence of  $G_R$  is given by an expression identical to that valid for  $G$  (see Sec. II E). From the last equation it is obvious that, at a given temperature, the coexistence condition of equal free energies of solid and liquid phases,  $G_s=G_l$ , implies also that the relative free energies are equal,  $G_{R,s}=G_{R,l}$ . The arbitrary zero of entropy is formally defined so that the relative free energy of ice,  $G_{R,s}$ , (and liquid water  $G_{R,l}$ ) is zero at the reference state point,  $(T_R, P_R)$ , for water molecules made of the isotope  $^1H$  with mass  $m_H$ ,

$$G_{R,s}(T_R, m_H) = G_{R,l}(T_R, m_H) \equiv 0. \quad (2)$$

Our task now is to find the coexistence condition for the other hydrogen isotopes at ambient pressure, i.e., the temperature,  $T_m$ , that satisfies equality in the free energies of both solid and liquid phases,

$$G_{R,s}(T_m, m_F) = G_{R,l}(T_m, m_F), \quad (3)$$

for an isotope mass,  $m_F$ , corresponding either to deuterium ( $m_D$ ) or tritium ( $m_T$ ) atoms.

### C. Isotope effect on the free energy

If temperature is held constant (say at the reference value  $T_R$ ), free energy differences as a function of the isotope mass are the same, whether calculated with  $G$  or  $G_R$  [see Eq. (1)]. Thus, for simplicity, our derivation is presented here by using  $G$  and omitting the indication of its  $T$  dependence. Assuming that the Gibbs free energy,  $G(m_H)$ , of a system made of the isotope  $^1\text{H}$  is known, then the unknown free energy,  $G(m_F)$ , of a system obtained by substituting  $^1\text{H}$  by the isotope of mass  $m_F$  can be calculated by the expression

$$G(m_F) = G(m_H) + \int_{m_H}^{m_F} \frac{\partial G(m_I)}{\partial m_I} dm_I. \quad (4)$$

We recall the thermodynamic relation between derivatives of the Gibbs free energy and the Hamiltonian,  $\hat{H}$ ,

$$\frac{\partial G(m_I)}{\partial m_I} = \left\langle \frac{\partial \hat{H}}{\partial m_I} \right\rangle_{NPT},$$

where the angle brackets represent an ensemble average. The Hamiltonian associated to the atomic nuclei in the water phase can be expressed as

$$\hat{H} = \hat{K}(m_O) + \hat{K}(m_I) + \hat{V} \quad (5)$$

where  $\hat{V}$  is the potential energy operator,  $\hat{K}(m_O)$  represents the sum of the KE operators of all the oxygen nuclei in the system, while  $\hat{K}(m_I)$  is the corresponding sum for the hydrogen isotopes. The mass dependence in the Hamiltonian operator appears only in the KE operator, thus

$$\left\langle \frac{\partial \hat{H}}{\partial m_I} \right\rangle_{NPT} = \left\langle \frac{\partial \hat{K}(m_I)}{\partial m_I} \right\rangle_{NPT} = - \frac{\langle \hat{K}(m_I) \rangle_{NPT}}{m_I} \quad (6)$$

where the last equality follows from the fact that the mass  $m_I$  appears in the KE operator as a  $m_I^{-1}$  factor.  $\langle \hat{K}(m_I) \rangle_{NPT}$  is the ensemble average of the sum of the KE of all the hydrogen isotopes in the system. This quantity is readily obtained in PI simulations by the virial estimator of the KE,  $K(m_I)$ . Inserting the last result into Eq. (4), one gets

$$G(m_F) = G(m_H) - \int_{m_H}^{m_F} \frac{\langle K(m_I) \rangle_{NPT}}{m_I} dm_I, \quad (7)$$

where  $\langle K(m_I) \rangle_{NPT}$  is the ensemble average of the virial KE estimator for the hydrogen isotope. The last equation shows that the change in the KE as a function of the isotope mass determines the free energy difference between two isotopes. We have implemented this free energy evaluation by the AS method.<sup>23</sup> The isotope mass,

$m_I$ , is changed from the initial value ( $m_H$ ) to the final one ( $m_F$ ) in a single non-equilibrium simulation. It is convenient to change the integration variable,  $m_I$ , to the dimensionless parameter,  $\lambda_I$ ,

$$\lambda_I = \frac{m_H}{m_I}, \quad (8)$$

so that the integration limits for  $\lambda_I$  are  $\lambda_H = 1$  and  $\lambda_F = m_H/m_F$ . For a simulation run consisting of a total number  $J$  of MDS, the actual value of the isotope mass,  $m_I$ , at the  $I$ 'th simulation step ( $I = 1, \dots, J$ ), is determined by substituting in Eq.(8) the following value of  $\lambda_I$

$$\lambda_I = 1 + (I - 1)\Delta\lambda, \quad (9)$$

where  $\Delta\lambda = (\lambda_F - \lambda_H)/(J - 1)$ . The Gibbs free energy as a function of the isotope mass  $m_I$ , is discretized for the simulation steps  $I > 1$  as

$$G(m_I) = G(m_{I-1}) + \frac{1}{2} \left( \frac{K(m_I)}{\lambda_I} + \frac{K(m_{I-1})}{\lambda_{I-1}} \right) \Delta\lambda, \quad (10)$$

where  $K(m_I)$  is the virial estimator of the KE of the hydrogen isotope at the simulation step  $I$ . The change of  $\lambda_I$  at each simulation step implies to update the corresponding isotope mass,  $m_I$ , as well as the spring constant for the harmonic coupling between beads of that isotope. A convenient application of the AS method is to perform two independent non-equilibrium simulations for a given free energy determination, where the initial and final integration limits are interchanged, so that the reversible path between the initial and final integration points is run in both directions. The free energy is then obtained as an average of these two independent runs.<sup>25,26</sup>

In the case of the  $NVT$  ensemble the mass dependence of the Helmholtz free energy,  $F$ , can be derived from the following relation analogous to Eq. (7)

$$F(m_F) = F(m_H) - \int_{m_H}^{m_F} \frac{\langle K(m_I) \rangle_{NVT}}{m_I} dm_I. \quad (11)$$

### D. Quantum-classical free energy difference

The previous derivation can be applied to calculate the free energy difference of a classical system with respect to its quantum limit at the reference state point ( $T_R, P_R$ ). The method implies the calculation of the reversible work associated to the following thermodynamic processes in the  $NPT$  ensemble: first (process A), the mass of the water molecules in the quantum system is increased, so that one formally reaches the limit of infinite molecular mass, where the classical limit becomes exact; second (process B), the mass of the water molecules is reduced back to its actual value but now considering that the system remains in its classical limit. The reversible work performed along

these two processes is the Gibbs free energy difference between the classical limit and the quantum system. This work can be calculated by Eq. (7) if applied to the particular case where the masses of all the atoms in the system are scaled by the same factor. It is convenient to define the variable  $\lambda$  as

$$\lambda = \frac{M_0}{M}, \quad (12)$$

where  $M_0$  and  $M$  are the actual and the scaled molecular masses of water, respectively. The relative Gibbs free energy difference,  $G_{R,cla}$ , of the classical limit with respect to the quantum system is then

$$G_{R,cla}(M_0) = \int_1^0 \left( \frac{\langle K(M) \rangle_{NPT}}{\lambda} - \frac{K_{cla}}{\lambda} \right) d\lambda. \quad (13)$$

The first summand in the integral determines the reversible work of process A, while the second summand corresponds to process B.  $\langle K(M) \rangle_{NPT}$  is the ensemble average of the virial estimator for the total KE (sum of oxygen and hydrogen atoms) for the quantum system where the molecular mass of water is  $M = M_0/\lambda$ .  $K_{cla}$  is the total KE in the classical limit that, as a consequence of the equipartition principle, is independent of the molecular mass  $M$  and depends only on temperature ( $k_B T/2$  per degree of freedom). The integral in Eq. (13) can be evaluated by the AS method, i.e., a PI simulation is performed where the molecular mass is slowly increased as a function of  $\lambda$ . The initial mass is  $M_0$  (set by  $\lambda = 1$ ) and the final mass is a large value defined by an adequate small  $\lambda_F$  (typically around 0.01). The value of  $G_{R,cla}$  must be then obtained by an extrapolation of the integral to the value  $\lambda_F \rightarrow 0$ , i.e.,

$$G_{R,cla} = \lim_{\lambda_F \rightarrow 0} I(\lambda_F), \quad (14)$$

where  $I(\lambda_F)$  is the definite integral in Eq. (13) when the upper integration limit is  $\lambda_F$  instead of zero. In Appendix A it is shown how the harmonic result for Eq. (13) let us expect that the extrapolation can be accurately done by a simple polynomial fit in the variable  $\lambda_F$ . An alternative calculation of the free energy,  $G_{R,cla}$ , is the method of Morales and Singer,<sup>44</sup> based on a thermodynamic integration that depends only on the potential energy. However, this method is not so convenient for the calculation of free energy differences between isotopes, as it would require to use the classical limit as an intermediate step to set up a reversible path connecting both isotopes.

### E. Temperature dependence of the free energy

The determination of the solid-liquid coexistence temperature requires to calculate the free energy of both

phases over an overlapping range of temperatures. To this aim we consider the following thermodynamic relation that relates the enthalpy,  $H(T)$ , with the Gibbs free energy

$$H(T) = \frac{\partial [\beta G(T)]}{\partial \beta}, \quad (15)$$

where  $\beta = 1/k_B T$  is the inverse temperature. Here, we have omitted the explicit indication of the pressure and mass dependence of  $G$  and  $H$ , that are assumed to be constant. Integrating this equation between the inverse reference temperature,  $\beta_R$ , and a final inverse temperature,  $\beta_F$ , one gets

$$\beta_F G(T_F) = \beta_R G(T_R) + \int_{\beta_R}^{\beta_F} d\beta H(T). \quad (16)$$

The RS method is implemented here by a non-equilibrium simulation where the inverse temperature is changed uniformly along a simulation run composed of  $J$  MDS as

$$\beta_i = \beta_R + (i-1)\Delta\beta, \quad (17)$$

where  $\beta_i$  is the inverse temperature of the  $i$ 'th simulation step ( $i = 1, \dots, J$ ) and the increment is  $\Delta\beta = (\beta_F - \beta_R)/(J-1)$ . The free energy at temperature  $T_i$  is discretized from Eq. (16) as

$$\beta_i G(T_i) = \beta_{i-1} G(T_{i-1}) + \Delta\beta \left[ \frac{H(T_i) + H(T_{i-1})}{2} \right]. \quad (18)$$

$H(T_i)$  is the system enthalpy at the  $i$ 'th simulation step. This expression corresponds to the  $NPT$  ensemble and is also valid if  $G$  is substituted by the relative energy  $G_R$ , because  $\beta G$  and  $\beta G_R$  differ only in a temperature-independent constant,  $S_0$  [see Eq. (1)]. The change of the inverse temperature  $\beta_i$  at each simulation step implies to update all variables that depend on temperature in our PI MD algorithm. These variables are the spring constants between beads, as well as the thermostat, barostat, and volume masses defined for the extended dynamics in the  $NPT$  ensemble.<sup>32-34</sup>

A relation equivalent to Eq. (18) can be derived in the  $NVT$  ensemble if  $G$  is substituted by the Helmholtz free energy,  $F$ , and the enthalpy,  $H$ , by the internal energy  $U$ .

## III. TEST SIMULATIONS

### A. Radial distribution function

The RDFs for OO, OH, and HH pairs have been calculated for water in the  $NVT$  ensemble at 298 K and

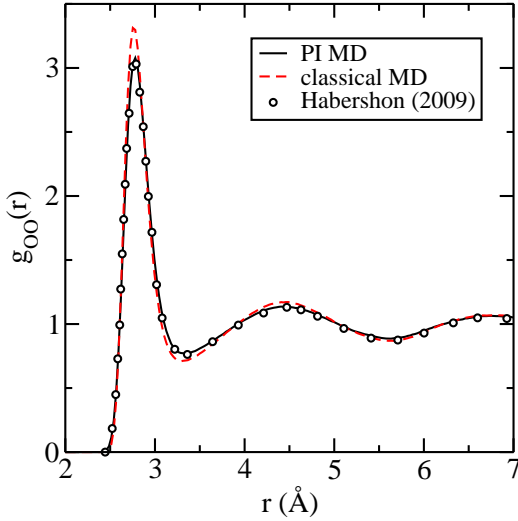


Figure 1: OO RDFs derived from quantum and classical simulations of water at 298 K and density  $0.997 \text{ g cm}^{-3}$ . For comparison the PI MD results of Ref. 12 are shown as open circles.

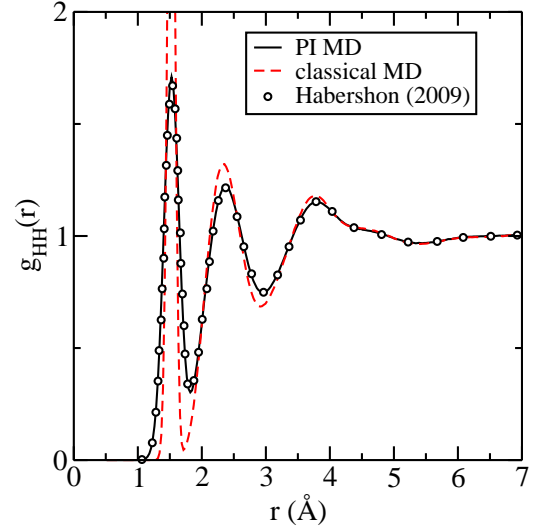


Figure 3: HH RDFs derived from quantum and classical simulations of water at 298 K and density  $0.997 \text{ g cm}^{-3}$ . For comparison the PI MD results of Ref. 12 are shown as open circles.

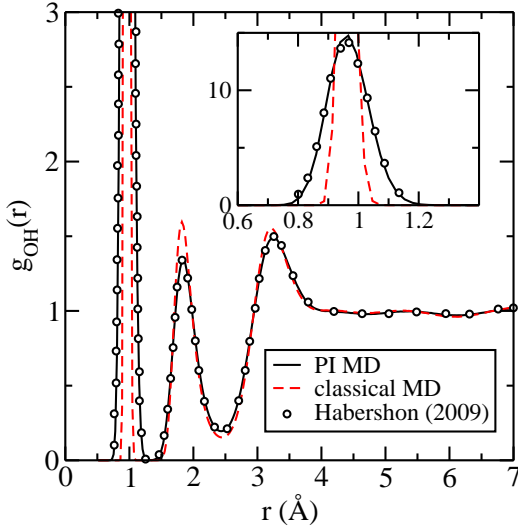


Figure 2: OH RDFs derived from quantum and classical simulations of water at 298 K and density  $0.997 \text{ g cm}^{-3}$ . For comparison the PI MD results of Ref. 12 are shown as open circles.

density  $0.997 \text{ g cm}^{-3}$ . The results of quantum and classical simulations are presented in Figs. 1 to 3. The curves were derived from runs composed of  $10^6$  MDS. Our quantum results have been compared to those published in Ref. 12. We observe in the three RDFs an excellent agreement between both sets of independent calculations. The technical setup of the simulations differs in many details, as the number of employed beads, the use of staging versus normal mode representations of the bead coordinates, the thermostats setup, the cut-

Table I: Molecular properties (bond distance, bond angle and dipole moment) as well as kinetic ( $K$ ) and potential energy ( $U_{pot}$ ) of liquid water at 298 K and density  $\rho = 0.997 \text{ g cm}^{-3}$ .  $r_{O...H}$  is the distance of the  $g_{OH}$  RDF maximum associated to the H-bond. The KE is partitioned into H-isotope and O-atom contributions ( $K_I$  and  $K_O$ , respectively).  $\rho_{TMD}$  is the maximum density of water at TMD, as derived from  $NPT$  simulations at  $P = 1 \text{ atm}$ . Both classical and quantum results are given. The quantum results correspond to normal ( $\text{H}_2\text{O}$ ), heavy ( $\text{D}_2\text{O}$ ), and tritiated ( $\text{T}_2\text{O}$ ) water.

	classical	$\text{T}_2\text{O}$	$\text{D}_2\text{O}$	$\text{H}_2\text{O}$	$\text{H}_2\text{O}^a$
$r_{O...H}$ (Å)	1.82	1.83	1.83	1.84	1.84
$\langle r_{OH} \rangle$ (Å)	0.963	0.972	0.974	0.977	-
$\langle \theta_{HOH} \rangle$ (deg)	104.8	104.8	104.7	104.7	-
$\langle \mu \rangle$ (D)	2.312	2.333	2.338	2.346	-
$\langle K \rangle$ (kcal mol $^{-1}$ )	2.68	5.78	6.51	8.13	-
$\langle K_I \rangle$ (kcal mol $^{-1}$ )	1.79	4.35	5.14	6.86	-
$\langle K_O \rangle$ (kcal mol $^{-1}$ )	0.89	1.43	1.37	1.27	-
$\langle U_{pot} \rangle$ (kcal mol $^{-1}$ )	-10.31	-7.13	-6.39	-4.57	-
TMD (K)	282(2)	-	-	280(2)	279(2)
$\rho_{TMD}$ (g cm $^{-3}$ )	1.004(2)	-	-	1.002(2)	1.001(2)

<sup>a</sup>Ref. [12]

off distance for short-range interactions, the approximation used to perform the Ewald summation in reciprocal space,<sup>12</sup> and the schemes used for the RESPA molecular dynamics. Therefore, the agreement found by the RDFs curves provides a check for the accuracy of the employed computational conditions.

The comparison of the RDFs obtained by PI simulations with the q-TIP4P/F model to experimental curves has been presented elsewhere<sup>12</sup> and will not be repeated

here. However, we focus here on differences found between quantum and classical limits of the RDFs of this model. The OO RDF curves in Fig. 1 show that classical water is more structured than in the quantum case. In the classical limit, the height of the first OO peak is larger and the position of the maximum is displaced by about 0.01 Å towards shorter OO distances. The second peak in the OH RDF curves in Fig. 2 corresponds to the H-bond distances. Controversial quantum and classical results have been published for this peak. A DFT study shows that in a quantum simulation this peak appears at shorter distances, which was interpreted as a hardening of the water structure with respect to classical simulations.<sup>45</sup> However, most simulations predict that quantum water is less structured than the classical counterpart.<sup>8</sup> Our quantum results for the q-TIP4P/F model show that this peak appears at a distance 0.02 Å larger than in the classical limit (see Table I), in agreement to the expectation that quantum corrections destabilize the H-bond network.

A comparison of other equilibrium results of quantum and classical water simulations is summarized in Table I. The quantum results have been derived for both normal, heavy and tritiated water. We see that quantum corrections associated to the atomic mass increase the intramolecular OH bond length by more than 0.01 Å, and the average molecular dipole moment,  $\langle\mu\rangle$ , by 1.5%. Note that this increase in  $\langle\mu\rangle$  is expected to act against the destabilization of the H-bond network, as the electrostatic interaction between neighboring water molecules becomes stronger. In Tab. I we also compare the average kinetic and potential energies of water. We note that the KE of normal water is 5.45 kcal mol<sup>-1</sup> larger in the quantum case. This increase is even larger for the potential energy (5.74 kcal mol<sup>-1</sup>) as a consequence of the anharmonicity of the model potential. A harmonic approximation predicts that both kinetic and potential energy increments must be identical. The partition of the KE between H- and O-atom contributions shows that the three-fold rise of the KE of normal water in the quantum case is mainly due to the H-atoms. For comparison we note that <sup>20</sup>Ne is the Lennard-Jones-type system whose atomic mass is closest to that of a water molecule. For solid <sup>20</sup>Ne at 24 K (a temperature close to the melting point at atmospheric pressure) the rise in KE amounts to a factor of about 1.4 with respect to the classical limit.<sup>46</sup>

### B. Temperature of maximum density

We have performed quantum and classical *NPT* simulations to calculate the temperature dependence of the water density,  $\rho$ , at ambient pressure. The results are summarized in Fig. 4. Our quantum results, shown by open circles, are again in reasonable agreement to the PI MD data of Ref. 12 for the same model potential. The densities calculated by both sets of independent simulations differ by not more than 0.5%, which is of the order of the estimated statistical error. A systematic deviation

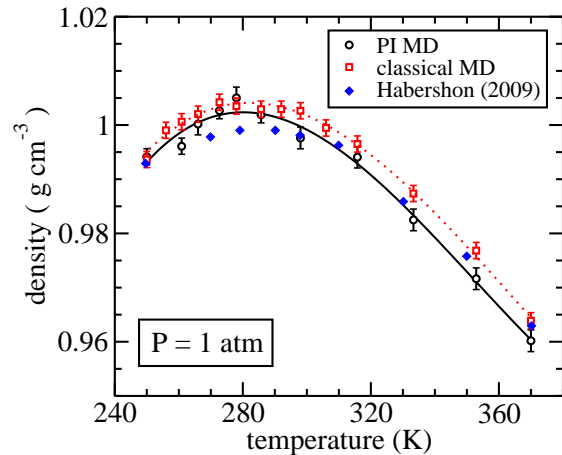


Figure 4: Density of water at 1 atm pressure obtained from classical and PI MD simulations. Lines are cubic polynomial fits to the simulation data.

is found at temperatures corresponding to the maximum density, indicating that the convergence over density fluctuations is particularly difficult in this region. The TMD, as obtained by a cubic polynomial fit to the simulation points, is found at 280 K, in good agreement to previously published results for this potential (see last two rows in Table I).<sup>12</sup> A comparison of simulation results to experiment has been presented elsewhere,<sup>12</sup> showing that the employed model provides realistic results. We recall that a proper description of the density of water is an important requirement for a water model to account for hydration effects.<sup>47</sup> The classical TMD is found at slightly higher temperature than in the quantum case, the shift amounts to 2 K, which is of the order of the statistical error. Classical and quantum temperature-density curves are so close that we have not tried to determine the hydrogen isotope effect in the TMD. However, we have checked that the density in simulations with tritiated water is, within the statistical error, very close to the normal water results. Therefore the employed q-TIP4P/F potential seems to be unable to reproduce the experimental isotope shift of the TMD in water.

The small difference between the classical and quantum TMD is consistent with the previous work of Habershon *et al.*<sup>12</sup> who found similar trends by comparing classical and quantum diffusion coefficients. A different result was derived for a rigid water model, TIP4PQ/2005. For this model, the classical TMD was found about 27 K higher than the quantum temperature, and the isotope effect for tritiated water amounts to 16 K, overestimating the experimental result of 9.4 K.<sup>18</sup> The main difference between the rigid TIP4PQ/2005 and the flexible q-TIP4P/F potential is the presence of an anharmonic intramolecular potential in the latter. The mechanism that has been previously used to explain the striking differences between quantum and classical diffusion coefficient of water when using either anharmonic or rigid

Table II: Relative free energies,  $G_R$ , of tritiated water at the reference point  $(T_R, P_R)$  as derived by independent AS simulations of different lengths. For a given simulation length two results are presented, corresponding to simulations where the initial and final integration limits  $(m_H, m_T)$  are interchanged. The last column shows the average of both independent runs.

MDS	$G_R$ (kcal mol <sup>-1</sup> )		
	$m_H \rightarrow m_T$	$m_T \rightarrow m_H$	average
$10^5$	-5.947	-5.950	-5.949
$2 \times 10^5$	-5.951	-5.949	-5.950
$4 \times 10^5$	-5.949	-5.951	-5.950
$1.5 \times 10^6$	-5.950	-5.952	-5.951

intramolecular models,<sup>12</sup> can be also used here to explain the differences found in the quantum and classical TMDs when using either anharmonic or rigid models. This mechanism implies the coupling between anharmonic intramolecular stretches (OH) and intermolecular H-bonds ( $O \cdots H$ ) in water. Anharmonic zero point effects weaken both  $O \cdots H$  and OH bonds (see the comparison of distances  $\langle r_{OH} \rangle$  and  $r_{O \cdots H}$  in Table I, quantum results are larger than classical ones). However, weakening of the OH bond increases the molecular dipole moment, that is accompanied by a concomitant strengthening of the intermolecular H-bond. Therefore, when quantum effects associated to the nuclear masses are included in an anharmonic flexible water potential, the H-bond is affected by competing factors acting in opposite directions, that might lead even to a mutual cancellation: *a*) weakening by zero point effects; *b*) strengthening by the increase of the molecular dipole moment. Obviously this competing mechanism is absent if the water model is rigid. Which of the two competing effects is dominant will depend on the details of the potential model and on the physical property under consideration. For the TMD of the q-TIP4P/F model, it seems that both competing effects cancel each other, leading to nearly identical quantum and classical curves of the liquid density as a function of temperature and then to a vanishingly small isotope effect in the TMD of water.

#### IV. ISOTOPE EFFECTS IN THE MELTING TEMPERATURE

##### A. D<sub>2</sub>O and T<sub>2</sub>O

To study the isotope effect in the melting temperature of ice we need first to calculate the relative free energies,  $G_R$ , of deuterated and tritiated phases at the reference state point  $(T_R, P_R)$ . To this aim we have performed AS simulations in the  $NPT$  ensemble according to Eq. (10). For the liquid phase, the dependence of  $G_R$  with the isotope mass is shown in Fig. 5. The convergence of  $G_R$  has been checked by comparing independent non-equilibrium simulations of different lengths for both solid

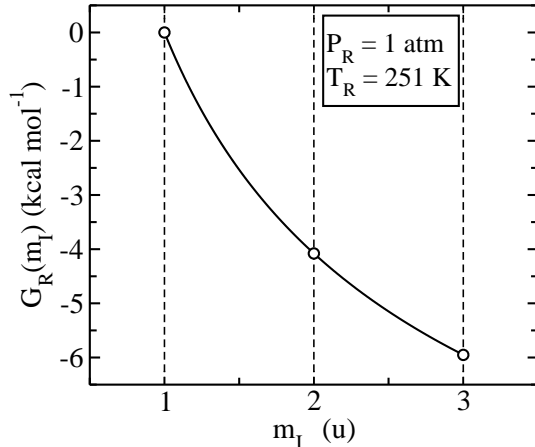


Figure 5: Relative free energy of liquid water as a function of the hydrogen isotope mass. The open circles corresponds to the masses of H, D, and T, respectively. The result was obtained by non-equilibrium simulations with the AS method at the reference state point  $(T_R, P_R)$ .

Table III: Relative free energy,  $G_R$ , at the reference point  $(T_R = 251$  K,  $P_R = 1$  atm) of solid and liquid phases of normal, heavy, and tritiated water.  $G_R$  is given in kcal mol<sup>-1</sup>, and its estimated error is  $\pm 0.001$  kcal mol<sup>-1</sup>. The last column summarizes the results obtained in the classical limit ( $G_{R,cla}$ ).

	H <sub>2</sub> O	D <sub>2</sub> O	T <sub>2</sub> O	classical limit
solid (s)	0	-4.108	-5.987	-8.912
liquid (l)	0	-4.079	-5.951	-8.875
$s - l$	0	-0.028	-0.036	-0.036

and liquid phases. This test is presented in Table II for tritiated water. We find that the statistical error in the free energy is even lower for heavy water and for the solid phases. Even with a modest number of simulation steps ( $J = 10^5$ ) the AS method shows reasonable convergence. Our final results for  $G_R$  are summarized in Table III, corresponding to non-equilibrium simulations with  $1.5 \times 10^6$  MDS for the liquid and  $4 \times 10^5$  MDS for the solid phases. For the heavier isotopes (D<sub>2</sub>O and T<sub>2</sub>O) the relative free energy of the solid at the reference state point is lower than in the liquid phase. This difference determines an isotope shift in the melting temperature, as temperature must be increased to restore the coexistence condition of equal free energy for both phases. The free energy difference between solid and liquid is larger for tritium than for deuterium, therefore the isotope shift in the melting temperature is expected to be larger for tritiated water than for deuterated water.

The temperature dependence of  $G_R$  has been calculated by RS simulations in the  $NPT$  ensemble [see Eq.(18)]. Several independent simulations of different lengths were performed to fix the conditions of adequate convergence for the non-equilibrium simulations. Again, each free energy estimation was based on two indepen-



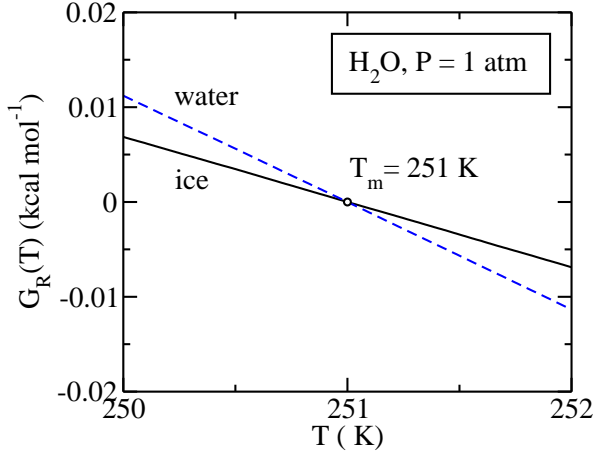


Figure 6: Relative free energy of normal water and ice at pressure of 1 atm as determined by our RS simulations. The melting point is  $T_m$ .

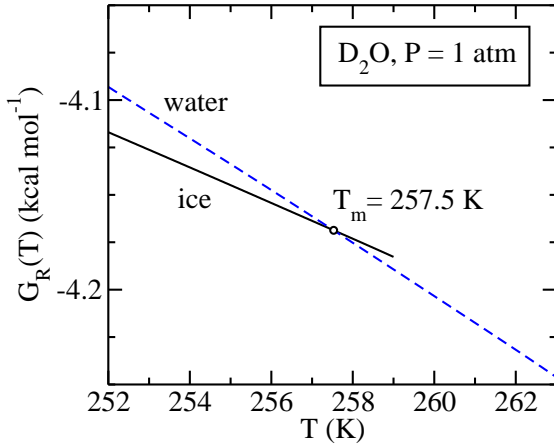


Figure 7: Relative free energy of deuterated water and ice at pressure of 1 atm as determined by our RS simulations. The melting point is  $T_m$ .

dent simulations where the integration limits of the temperature in the reversible path were interchanged, and the final results were obtained as an average of both RS simulations. The employed computational conditions (integration limits for the temperature and number of MDS) used in our RS simulations are summarized in Table IV. The liquid RS simulations require typically simulation lengths one order of magnitude larger than the solid phase. The  $G_R(T)$  results obtained for normal, deuterated and tritiated phases are presented in Figs. 6-8. The condition of equal free energy of the solid and liquid phases determines the melting point at ambient pressure. The melting temperature is shifted towards

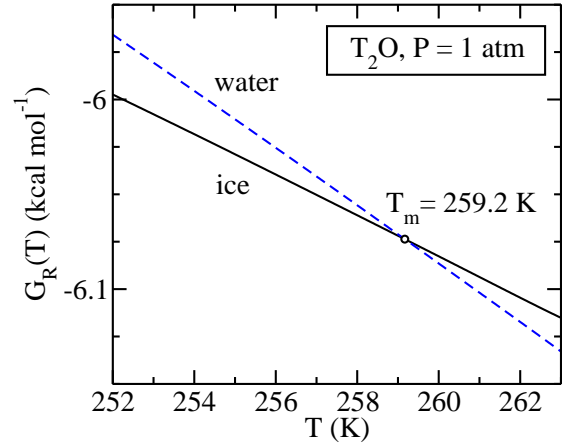


Figure 8: Relative free energy of tritiated water and ice at pressure of 1 atm as determined by our RS simulations. The melting point is  $T_m$ .

Table IV: Computational conditions used in the non-equilibrium RS simulations to determine the temperature dependence of the relative Gibbs free energy of the studied isotope compositions of water and ice.

isotope	phase	$T$ range (K)	MDS
H <sub>2</sub> O	liquid	250-252	$2 \times 10^5$
H <sub>2</sub> O	solid	250-252	$5 \times 10^4$
D <sub>2</sub> O	liquid	251-263	$2 \times 10^6$
D <sub>2</sub> O	solid	251-259	$2 \times 10^5$
T <sub>2</sub> O	liquid	251-263	$2 \times 10^6$
T <sub>2</sub> O	solid	251-263	$2 \times 10^5$
classical	liquid	251-261	$3 \times 10^6$
classical	solid	251-273	$8 \times 10^5$

higher values as the hydrogen isotope mass increases. The estimated isotope shift in the melting temperature is  $6.5 \pm 0.5$  K for heavy water and  $8.2 \pm 0.5$  K for tritiated water for the q-TIP4P/F model. Experimental isotope shifts amount to 3.8 K and 4.5 K, respectively. Thus, the q-TIP4P/F model overestimates the isotope shift in the melting temperature of ice. This result contrasts with the nearly absence of isotope shifts in the TMD of water, as predicted by the same potential.

Melting in atomic solids can be thought of as being controlled by the local vibrations of the atoms. The Lindemann criterion presents a threshold for the maximum amplitude of atomic vibrations that can be sustained by the crystal. At the melting point of ice we find that this amplitude is similar for both O- and H-atoms and amounts to about 6% of the H-bond distance.

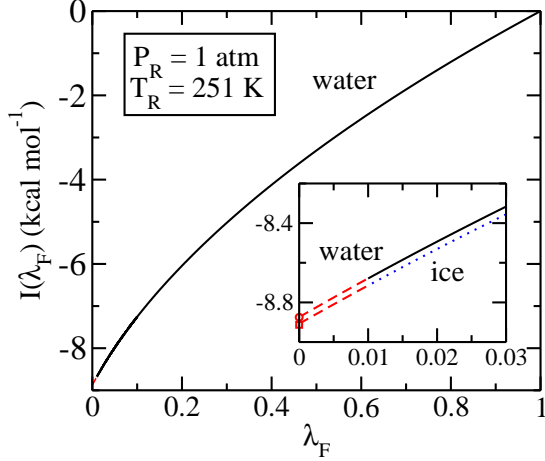


Figure 9: The function  $I(\lambda_F)$  obtained for liquid water by non-equilibrium AS  $NPT$  simulations at the reference state point  $(T_R, P_R)$ . The extrapolation  $\lambda_F \rightarrow 0$  is shown for the solid and liquid phases in the inset of the figure.

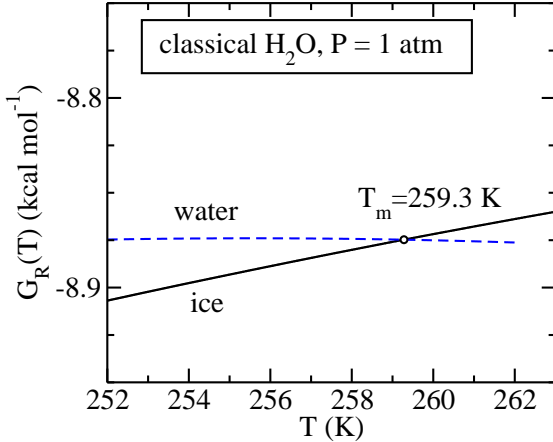


Figure 10: Relative free energy of water and ice at pressure of 1 atm as determined by our RS simulations in the classical limit. The melting point is  $T_m$ .

### B. Classical limit

The determination of the classical melting point implies to calculate the relative free energy,  $G_{R,cla}$ , of the classical limit of water and ice with respect to the quantum case at the reference state point. To this aim we have performed AS simulations where the molecular mass of water is slowly changed from its normal value,  $M_0$ , to an arbitrary large value,  $M_F$ , determined by the parameter

$\lambda_F = M_0/M_F$ . The function  $I(\lambda_F)$  introduced in Sec. IID [see Eq. (14)] is then obtained by a discretization of the integral given in Eq. (13) as a running average along the non-equilibrium simulation. The AS results in the solid phase have been derived with  $4 \times 10^5$  MDS while the liquid phase required longer runs of  $1.6 \times 10^6$  MDS. As usual in our non-equilibrium simulations, two independent simulation runs were performed by interchanging the integration limits, and the final free energy is the average of these two runs. The function  $I(\lambda_F)$  for the liquid phase is shown in Fig. 9. The inset in the figure shows the result of the extrapolation  $\lambda_F \rightarrow 0$  for both solid and liquid phases. The extrapolated values are summarized in the last column of Table III. These figures were obtained by a polynomial fit of  $I(\lambda_F)$ , after checking that the extrapolation is reasonably stable against both the polynomial degree and the  $\lambda_F$  interval employed in the numerical fit. The results given in Table III were derived by a 10'th degree polynomial fit in the  $\lambda_F$  range  $[0.01, 0.2]$ . Somewhat surprising is that the difference between the relative free energy of the solid and liquid phases in the classical limit is, within the statistical error, identical to the value found for tritiated phases. This fact will be relevant for the melting temperature of the classical system.

The temperature dependence of the relative free energy of water and ice at ambient pressure is presented in Fig. 10 for the classical limit. The computational conditions for the non-equilibrium RS simulations were summarized in the last two rows of Table IV. The estimated classical melting point is  $259.3 \pm 0.5$  K. We find again an excellent agreement to the result reported by Habershon *et al.*<sup>12</sup> of  $259 \pm 1$  K. Note that both classical melting temperatures were determined by different methods, i.e., by direct coexistence simulations<sup>12</sup> and by free energy calculations. An advantage of the free energy method is that other important physical quantities are readily available, which is not the case by a direct coexistence method.

In Table V we summarize the simulation results of several melting properties for the studied isotopic compositions of water and also in the classical limit. The melting entropy,  $\Delta S_m$ , was estimated from the numerical temperature derivative of the Gibbs free energy curves given in Figs. 6-8 and 10 at coexistence conditions, while the melting enthalpy was calculated by two independent ways: (a) as  $T_m \Delta S_m$ ; (b) by direct calculation of the solid and liquid enthalpies by  $NPT$  simulations at coexistence conditions. The agreement between both methods provides evidence about the internal consistency of our results. The isotope effect in the melting entropy and enthalpy is low, practically within the statistical uncertainty of our results. The employed water model underestimates both the experimental values of the melting entropy and enthalpy. At coexistence conditions the negative sign in the change of the KE upon melting indicates that the KE of ice is larger than that of the liquid phase.

Table V: Melting temperature, entropy and enthalpy for normal, heavy, and tritiated water as well as classical limit results at ambient pressure. The melting enthalpy was estimated by two independent methods. The change in the kinetic and potential energy upon melting (liquid minus solid values) and the molar volume ( $V_m$ ) of the solid and liquid phases are also given. The standard error in the final digits is given in parenthesis.

	classical	T <sub>2</sub> O	D <sub>2</sub> O	H <sub>2</sub> O	exp. H <sub>2</sub> O
$T_m$ (K)	259.3(5)	259.2(5)	257.5(5)	251	273.15
$\Delta S_m$ (cal mol <sup>-1</sup> K <sup>-1</sup> )	4.52(5)	4.45(5)	4.52(5)	4.40(5)	5.3
$\Delta H_m^a$ (kcal mol <sup>-1</sup> )	1.17(2)	1.15(2)	1.16(2)	1.10(2)	1.44
$\Delta H_m^b$ (kcal mol <sup>-1</sup> )	1.18(3)	1.10(3)	1.13(3)	1.07(3)	1.44
$\Delta K_m$ (kcal mol <sup>-1</sup> )	0	-0.024(5)	-0.038(5)	-0.078(5)	
$\Delta U_{pot}$ (kcal mol <sup>-1</sup> )	1.18(3)	1.12(3)	1.17(3)	1.14(3)	
$V_{m,s}$ (cm <sup>3</sup> mol <sup>-1</sup> )	19.40(1)	19.47(1)	19.49(1)	19.56(1)	19.66
$V_{m,l}$ (cm <sup>3</sup> mol <sup>-1</sup> )	17.99(6)	18.15(6)	18.03(6)	17.96(6)	18.02
$\Delta V_m$ (cm <sup>3</sup> mol <sup>-1</sup> )	-1.41(6)	-1.32(6)	-1.46(6)	-1.60(6)	-1.64

<sup>a</sup>from  $T_m \Delta S_m$

<sup>b</sup>from independent solid and liquid *NPT* simulations at coexistence conditions

At room temperature the KE of tritium in tritiated water is a factor about 2.4 times larger than in the classical limit (see Table I), i.e., although tritium is three times heavier than hydrogen, quantum effects related to its nuclear mass are still significant below room temperature. Therefore an unexpected result of the employed model potential is that the classical melting point is nearly identical to that one found for tritiated water, and the reason for this behavior will be investigated in the next subsection.

### C. Kinetic energy and molecular mass

We have already seen that isotope shifts in the melting point are caused by the fact that the free energy of the solid and liquid phases changes by different amounts as the isotopic mass changes. This is a quantum effect related to the atomic mass, as in the classical limit the mass dependence of the free energy is identical for both phases. To understand the shift found in the melting temperature in the classical limit, it is interesting to study the difference between the Gibbs free energy of the solid and liquid phases as a function of the scaled molecular mass,  $M_F$ , as determined by the parameter  $\lambda_F = M_0/M_F$ . This difference is given by an expression similar to Eq. (13)

$$G_{R,s}(M_F) - G_{R,l}(M_F) = \int_1^{\lambda_F} \left( \frac{\langle K_s(M) \rangle_{NPT}}{\lambda} - \frac{\langle K_l(M) \rangle_{NPT}}{\lambda} \right) d\lambda. \quad (19)$$

The instantaneous values of the virial KE estimators of the integrand are available from the non-equilibrium AS simulations used to calculate Fig. 9. These values have been used to plot the solid-liquid Gibbs free energy difference as a function of the inverse molecular mass,  $M_F^{-1}$ , in Fig. 11. This curve is not a monotonous function but

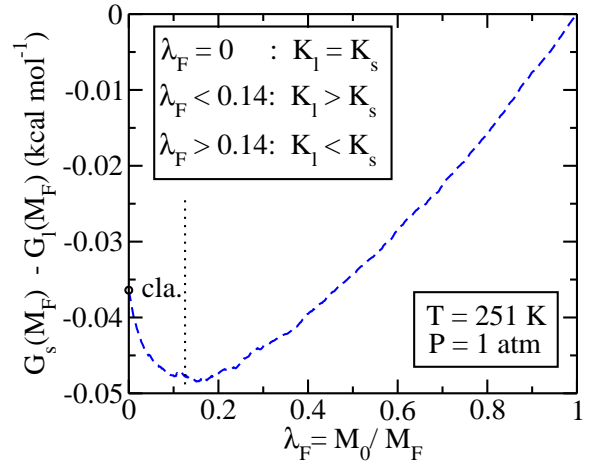


Figure 11: Gibbs free energy difference between ice and water as a function of the molecular mass at the reference state point ( $T_R, P_R$ ). Depending on the molecular mass the KE of the liquid ( $K_l$ ) may be larger than that of the solid ( $K_s$ ).

it displays a minimum for a molecular mass defined by the parameter  $\lambda_F \sim 0.14$ . This minimum makes that the free energy difference in the classical limit (corresponding to  $\lambda_F = 0$ , open circle in Fig. 11) is similar to that obtained for tritiated phases (see Table III), and therefore the classical melting point is found at nearly the same temperature as for T<sub>2</sub>O. If the curve in Fig. 11 were a monotonous decreasing function up to  $\lambda_F = 0$  (i.e., without the presence of a minimum), then the classical absolute value of the free energy difference between the two phases should be larger than for T<sub>2</sub>O, and therefore the classical melting temperature should also increase with respect to the tritiated phase.

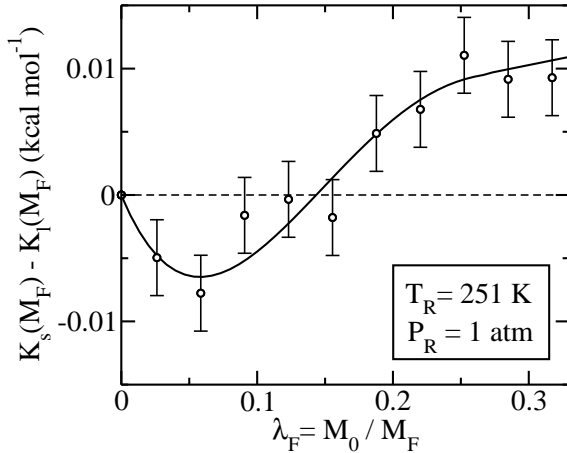


Figure 12: Kinetic energy difference between ice and water as a function of the molecular mass at the reference state point ( $T_R, P_R$ ). The line is a guide to the eye.

The existence of a minimum in the function given in Fig. 11 is related to a change in the sign of the integrand of Eq. (19) in the region around the minimum. This fact is clearly seen by plotting in Fig. 12 the difference between the KE of solid and liquid phases as a function of the inverse molecular mass,  $M_F^{-1}$ , at the reference state point. We find that when the molecular mass is large ( $\lambda_F < 0.14$ , or  $M_F > 7M_0$ ) the KE of water is larger than that of ice, while the opposite behavior is found for lower molecular masses ( $\lambda_F > 0.14$ ). The physical origin of this apparently complicate behavior of the KE is related to the presence of the two types of bonds in the water phases: intramolecular OH pairs and intermolecular H-bonds. The H-bond network is stronger in ice than in water, as a result of the higher molecular disorder in the liquid, which implies that vibrational frequencies of H-bonds are larger in ice than in water. On the contrary, the OH stretch frequency in the liquid is higher than in the solid. In Fig. 13 we display the OH distance for water and ice as a function of the molecular mass at the reference state point. For all molecular masses, the OH distance is lower for water than for ice, a fact that implies also a higher vibrational OH stretch frequency in water. This behavior is illustrated by the inset in Fig. 13 that displays the increase of the quasi-harmonic stretch frequency  $\omega_{OH}$  for the employed q-TIP4P/F potential as the OH distance decreases.

In the classical limit, corresponding to  $\lambda_F = 0$  (infinite molecular mass), all modes have the same KE (equipartition principle) and the KE difference between ice and water vanishes. In the case of large, but finite, molecular mass ( $0 < \lambda_F < 0.14$ ), the KE difference is determined by the modes with highest vibrational frequencies, i.e., the OH stretches. The reason is that the leading quantum correction for vibrational modes, as the molecular mass decreases, corresponds to those modes that satisfy that their energy quantum is larger than the thermal en-

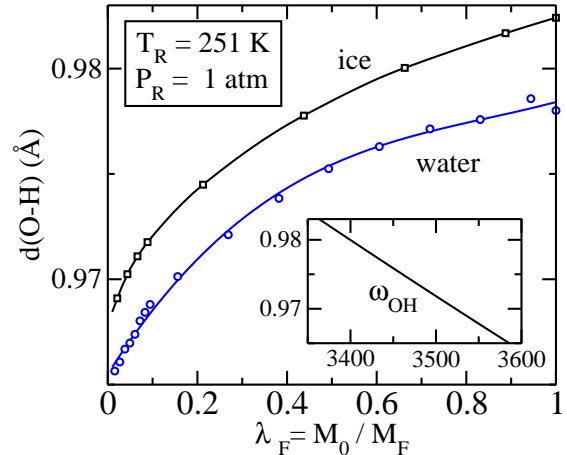


Figure 13: Intramolecular OH distance of ice and water as a function of the molecular mass at the reference state point ( $T_R, P_R$ ). Lines are guides to the eye. The inset shows the quasi-harmonic stretch frequency  $\omega_{OH}$  (in  $\text{cm}^{-1}$ ) as a function of the OH distance for the q-TIP4P/F potential.  $\omega_{OH}$  was derived from the second derivative of the potential energy with respect to the OH bond distance and by considering the actual O and H masses.

ergy,  $\hbar\omega > k_B T_R$ , and this condition will be first met for the modes with highest frequency (OH stretches). Thus, for large molecular masses with  $\lambda_F < 0.14$ , the KE of water results larger than that of ice, as the stretch frequencies  $\omega_{OH}$  are larger in the liquid. For smaller molecular masses ( $\lambda_F > 0.14$ ), the quantum behavior of the vibrational modes associated to H-bonds becomes important. For H-bonds related modes, the KE is larger in ice than in water, as their vibrational frequencies are higher in ice. The effect of the H-bonds dominates over the OH stretches for  $\lambda_F > 0.14$  in the sense that the KE of ice results larger than that of water.

The shorter OH distance in liquid water is a consequence of the coupling between OH stretches and H-bonds. Since the H-bond network in water is weaker than in ice, then the intramolecular OH bonds become shorter. A recent Compton scattering study of water versus ice Ih arrives to the same conclusion: an elongation of the H-bond in water leads to a systematic shortening of the intramolecular OH bond, and the OH bond in water is about 0.01 Å shorter than in ice.<sup>48</sup>

## V. CONCLUSIONS

In the present work we have used free energy techniques to study the isotope shift in the melting temperature of ice Ih. The employed AS and RS methods are based on algorithms where the Hamiltonian or a state variable are adiabatically changed along a simulation run. The reversible work associated to this change is equal to the free energy difference between the initial and final

state, as long as the change is performed slowly (adiabatically). These free energy algorithms are easily implemented in any code prepared for equilibrium simulations.

Our PI simulations of water have been done with the q-TIP4P/F model, a point charge potential that includes an anharmonic treatment of molecular flexibility. Several equilibrium properties (RDFs, liquid density as a function of temperature) have been compared to results previously published for this potential. The agreement found between independent simulations provides a check for the employed computational method and simulation conditions.

We have found that the experimental isotope effect in the TMD of water is not correctly described by the employed potential. In fact, the TMD calculated in the classical limit is very close to the quantum value. Quantum effects associated to the atomic mass activate a competing mechanism that produces a weakening of the H-bond through quantum zero point fluctuations, but also a strengthening of the same H-bonds by the increase in the molecular dipole moment of water molecules, that is found in the quantum simulations. Although this competing mechanism, previously observed by Habershon *et al.*<sup>12</sup> to explain the trends in the classical and quantum diffusion coefficients, seems to be a real physical effect, its influence in a given physical property depends on the details of the anharmonic flexible water potential, so that a small imbalance between both competing factors might lead to an unphysical result. This seems to be the case for the isotope effect in the TMD of water.

The isotope effect in the melting temperature at ambient pressure of ice has been determined by the calculation of the Gibbs free energy as a function of the isotope mass and temperature. We find that the isotope effect predicted by the q-TIP4P/F potential ( $6.5 \pm 0.5$  K and  $8.2 \pm 0.5$  K for heavy and tritiated water, respectively) are larger than the experimental values (3.8 K and 4.5 K, respectively). An unexpected result is that the classical melting point at 1 atm is nearly identical to the one obtained for tritiated water. We have shown that this behavior is related to the fact that the OH stretches in water display a higher frequency than in the solid phase. It is clear that the employed q-TIP4P/F potential is not able to quantitatively predict the isotope effect in the melting temperature of ice, but it has helped to identify that the coupling between molecular flexibility and the H-bond network may have significant implications in the phase behavior of water.

### Acknowledgments

This work was supported by Ministerio de Ciencia e Innovación (Spain) through Grant No. FIS2009-12721-C04-04 and by Comunidad Autónoma de Madrid through project MODELICO-CM/S2009ESP-1691. The authors

benefited from discussions with L. M. Sesé, C. Vega, E.G. Noya, and E. R. Hernández.

### Appendix A: Extrapolation of $G_{R,cla}$

The largest deviation between a quantum and classical treatment of a water phase (either solid or liquid) is expected to be due to those vibrational modes of highest frequency (i.e., intramolecular OH stretches and H-bonds). A harmonic treatment of these modes gives useful information on the analytical behavior of the definite integral in Eq. (19) when the upper integration limit vanishes ( $\lambda_F \rightarrow 0$ ). Note that the limit  $\lambda_F = 0$  is not accessible numerically as it would correspond to an infinite mass. Let us assume a simple one-dimensional harmonic oscillator defined by a wavenumber  $\omega_0$  and mass  $M_0$ . The oscillator mass depends on the integration parameter  $\lambda$  as  $M = M_0/\lambda$ , while the oscillator wavenumber varies as  $\omega = \omega_0 \lambda^{1/2}$ . The thermal expectation value of the KE of the quantum oscillator for a given  $\lambda$  is given by

$$\langle K \rangle = K_0 \lambda^{1/2} \coth \left( \frac{K_0}{K_{cla}} \lambda^{1/2} \right), \quad (\text{A1})$$

where  $K_{cla}$  is the classical KE

$$K_{cla} = \frac{1}{2} k_B T, \quad (\text{A2})$$

and  $K_0$  is the zero-point KE

$$K_0 = \frac{\hbar \omega_0}{4}. \quad (\text{A3})$$

By a Taylor expansion of the r.h.s. of Eq.(A1), the integrand of Eq. (13) for a harmonic mode can be written as

$$\frac{\langle K \rangle - K_{cla}}{\lambda} = \frac{K_0^2}{K_{cla}} - \frac{K_0^4}{K_{cla}^3} \lambda + O(\lambda^2). \quad (\text{A4})$$

The definite integral given in Eq. (13) must be obtained by numerical extrapolation of  $I(\lambda_F)$  to the  $\lambda_F = 0$  limit [see Eq. (14)]. The harmonic result for the integrand in Eq. (A4) suggests that a polynomial fit for  $I(\lambda_F)$  is a convenient numerical way to obtain the desired extrapolation. As the employed q-TIP4P/F potential is anharmonic, we do not expect to assign any particular meaning to the fitted coefficients.

- <sup>1</sup> J. R. Petit, J. Jouzel, D. Raynaud, N. I. Barkov, J.-M. Barnola, I. Basile, M. Bender, J. Chappellaz, M. Davis, G. Delaygue, et al., *Nature* **399**, 429 (1999).
- <sup>2</sup> J. A. Barker and R. O. Watts, *Chem. Phys. Lett.* **3**, 144 (1969).
- <sup>3</sup> A. Rahman and F. H. Stillinger, *J. Chem. Phys.* **55**, 3336 (1971).
- <sup>4</sup> M. W. Mahoney and W. L. Jorgensen, *J. Chem. Phys.* **115**, 10758 (2001).
- <sup>5</sup> W. L. Jorgensen and J. Tirado-Rives, *PNAS* **102**, 6665 (2005).
- <sup>6</sup> C. McBride, C. Vega, E. G. Noya, R. Ramírez, and L. M. Sesé, *J. Chem. Phys.* **131**, 024506 (2009).
- <sup>7</sup> M. V. Fernández-Serra and E. Artacho, *Phys. Rev. Lett.* **96**, 016404 (2006).
- <sup>8</sup> J. A. Morrone and R. Car, *Phys. Rev. Lett.* **101**, 017801 (2008).
- <sup>9</sup> S. Yoo, X. C. Zeng, and S. S. Xantheas, *J. Chem. Phys.* **130**, 221102 (2009).
- <sup>10</sup> C. Vega, E. Sanz, and J. L. F. Abascal, *J. Chem. Phys.* **122**, 114507 (2005).
- <sup>11</sup> J. L. F. Abascal and C. Vega, *J. Chem. Phys.* **123**, 234505 (2005).
- <sup>12</sup> S. Habershon, T. E. Markland, and D. E. Manolopoulos, *J. Chem. Phys.* **131**, 024501 (2009).
- <sup>13</sup> F. Paesani, W. Zhang, D. A. Case, T. E. Cheatham, III, and G. A. Voth, *J. Chem. Phys.* **125**, 184507 (2006).
- <sup>14</sup> R. Ludwig and F. Weinhold, *Phys. Chem. Chem. Phys.* **2**, 1613 (2000).
- <sup>15</sup> R. A. Kuharski and P. J. Rossky, *J. Chem. Phys.* **82**, 5164 (1985).
- <sup>16</sup> G. S. D. Buono, P. J. Rossky, and J. Schnitker, *J. Chem. Phys.* **95**, 3728 (1991).
- <sup>17</sup> H. A. Stern and B. J. Berne, *J. Chem. Phys.* **115**, 7622 (2001).
- <sup>18</sup> E. G. Noya, C. Vega, L. M. Sesé, and R. Ramírez, *J. Chem. Phys.* **131**, 124518 (2009).
- <sup>19</sup> L. H. de la Peña and P. G. Kusalik, *J. Chem. Phys.* **121**, 5992 (2004).
- <sup>20</sup> F. Paesani, S. Iuchi, and G. A. Voth, *J. Chem. Phys.* **127**, 074506 (2007).
- <sup>21</sup> M. Shiga and W. Shinoda, *J. Chem. Phys.* **123**, 134502 (2005).
- <sup>22</sup> C. Vega, M. M. Conde, C. McBride, J. L. F. Abascal, E. G. Noya, R. Ramirez, and L. M. Sesé, *J. Chem. Phys.* **132**, 046101 (2010).
- <sup>23</sup> M. Watanabe and W. P. Reinhardt, *Phys. Rev. Lett.* **65**, 3301 (1990).
- <sup>24</sup> M. de Koning, A. Antonelli, and S. Yip, *Phys. Rev. Lett.* **83**, 3973 (1999).
- <sup>25</sup> R. Ramírez, C. P. Herrero, A. Antonelli, and E. R. Hernández, *J. Chem. Phys.* **129**, 064110 (2008).
- <sup>26</sup> R. Ramírez and C. P. Herrero, *J. Chem. Phys.* **129**, 204502 (2008).
- <sup>27</sup> R. P. Feynman, *Statistical Mechanics* (Addison-Wesley, New York, 1972).
- <sup>28</sup> M. J. Gillan, *Phil. Mag. A* **58**, 257 (1988).
- <sup>29</sup> D. M. Ceperley, *Rev. Mod. Phys.* **67**, 279 (1995).
- <sup>30</sup> C. Chakravarty, *Int. Rev. Phys. Chem.* **16**, 421 (1997).
- <sup>31</sup> G. J. Martyna, M. E. Tuckerman, D. J. Tobias, and M. L. Klein, *Mol. Phys.* **87**, 1117 (1996).
- <sup>32</sup> G. J. Martyna, A. Hughes, and M. E. Tuckerman, *J. Chem. Phys.* **110**, 3275 (1999).
- <sup>33</sup> M. E. Tuckerman, in *Quantum Simulations of Complex Many-Body Systems: From Theory to Algorithms*, edited by J. Grotendorst, D. Marx, and A. Muramatsu (NIC, FZ Jülich, 2002), p. 269.
- <sup>34</sup> M. E. Tuckerman and A. Hughes, in *Classical & Quantum Dynamics in Condensed Phase Simulations*, edited by B. J. Berne and D. F. Coker (World Scientific, New Jersey, 1998), p. 311.
- <sup>35</sup> P. Pacheco, *Parallel Programming with MPI* (Morgan-Kaufmann, San Francisco, 1997).
- <sup>36</sup> V. Buch, P. Sandler, and J. Sadlej, *J. Phys. Chem. B* **102**, 8641 (1998).
- <sup>37</sup> J. K. Johnson, J. A. Zollweg, and K. E. Gubbins, *Mol. Phys.* **78**, 591 (1993).
- <sup>38</sup> M. F. Herman, E. J. Bruskin, and B. J. Berne, *J. Chem. Phys.* **76**, 5150 (1982).
- <sup>39</sup> M. Parrinello and A. Rahman, *J. Chem. Phys.* **80**, 860 (1984).
- <sup>40</sup> R. Ramírez, C. P. Herrero, E. R. Hernández, and M. Cardona, *Phys. Rev. B* **77**, 045210 (2008).
- <sup>41</sup> J. G. Kirkwood, *J. Chem. Phys.* **3**, 300 (1935).
- <sup>42</sup> M. P. Allen and D. J. Tildesley, *Computer Simulation of Liquids* (Clarendon Press, Oxford, 1987).
- <sup>43</sup> D. Frenkel and B. Smit, *Understanding Molecular Simulation* (Academic Press, San Diego, 1996).
- <sup>44</sup> J. J. Morales and K. Singer, *Mol. Phys.* **73**, 873 (1991).
- <sup>45</sup> B. Chen, I. Ivanov, M. L. Klein, and M. Parrinello, *Phys. Rev. Lett.* **91**, 215503 (2003).
- <sup>46</sup> C. P. Herrero, *Phys. Rev. B* **65**, 014112 (2001).
- <sup>47</sup> D. Paschek, *J. Chem. Phys.* **120**, 6674 (2004).
- <sup>48</sup> K. Nygård, M. Hakala, S. Manninen, A. Andrejczuk, M. Itou, Y. Sakurai, L. G. M. Pettersson, and K. Hämmäläinen, *Phys. Rev. E* **74**, 031503 (2006).